Determination of the liquidus and solidus temperatures of FeCrAl stainless steel

Zhi-biao Han, Jian-hua Liu, Yang He, Kang-wei Li, Yi-long Ji, and Jian Liu

Research Institute of Metallurgy Engineering, University of Science and Technology Beijing, Beijing 100083, China

Abstract: The liquidus and solidus temperatures of FeCrAl stainless steel were determined by differential scanning calorimetry (DSC) at different heating rates. They were also calculated by Thermo-calc software and empirical formulae separately. The accuracy of calculation results was assessed by comparison with the corresponding DSC results. The liquidus temperatures calculated by empirical formulae, which exhibited a maximum deviation of 8.6°C, were more accurate than those calculated using Thermo-calc, which exhibited a maximum deviation of 12.11°C. On the basis of Thermo-calc calculations performed under the Scheil model, the solidus temperature could be well determined from solid fraction (f_S) vs. temperature (t) curves at $f_S = 0.99$. Furthermore, a theoretical analysis to determine the solidus temperature with this method was also provided.

Keywords: ferritic stainless steel; liquidus temperature; solidus temperature; differential scanning calorimetry

1. Introduction

FeCrAl stainless steel is ferritic stainless steel with high Cr and Al contents. Because of its excellent resistance to oxidation at high temperatures, it was originally used in heating applications [1−2]. With the boom of automobile industry, it was gradually adopted as an ideal material for automobile exhaust purifier carriers because of its relatively low thermal expansivity and low heat capacity [3−4].

The liquidus and solidus temperatures, t_L and t_S, are critical parameters in the study of solidification features and the formation mechanism of solidification structures. However, determining the liquidus and solidus temperatures for FeCrAl stainless steel, especially the solidus temperature, is not easy.

Dynamic calorimeter methods, such as differential scanning calorimetry (DSC) and differential thermal analysis (DTA), are recognized as the best approach to determine solidus and liquidus temperatures [5−6]. Thermodynamic software programs such as Thermo-cacl (TC) and Fact-sage are capable of determining the liquidus temperature but not

the solidus temperature. Furthermore, for systems beyond the scope of the software databases, assessments and rectifications by other means (DSC or DTA) are strongly recommended to avoid significant deviations. Iron-based ternary phase diagrams that are applicable to stainless steels are not complete [7−8], and therefore may not be helpful in determining the liquidus and solidus temperatures of FeCrAl stainless steel. Empirical formulae could also be used to obtain liquidus and solidus temperatures; however, in the case of FeCrAl stainless steel, results obtained using these formulae should also be verified by experimental DSC or DTA results [9].

In this paper, the liquidus and solidus temperatures of FeCrAl stainless steel were calculated using the TC software and empirical formulae, respectively. The results obtained using these two approaches were then separately compared with results obtained by DSC, which led to our development of a better method for calculating the liquidus of FeCrAl stainless steel. On the basis of the solidus temperature obtained by DSC and that obtained from the solid fraction (f_S) vs. temperature (t) curve calculated using TC under the Scheil model, a method for obtaining the solidus tempera-

Corresponding author: Jian-hua Liu   E-mail: liujianhua@metall.ustb.edu.cn

ⓩ Springer

1142

Int. J. Miner. Metall. Mater., *Vol. 22, No. 11, Nov. 2015*

ture by TC was introduced and theoretically analyzed.

2. DSC testing to determine T_L and T_S

2.1. Sample preparation

FeCrAl stainless steel is ferritic stainless steel with high Cr and Al contents. The typical composition of commercial FeCrAl stainless steel is listed in Table 1.

As is shown in Table 1, commercial FeCrAl stainless steel usually contains 3wt%−6wt% [Al], 18wt%−21wt% [Cr], 0.003wt%−0.03wt% [C] as well as other impurities. Accordingly, four melts of 20 kg FeCrAl stainless steel ingots were prepared using a vacuum induction furnace and the surfaces of the ingots were subsequently polished. The positions from where scraps as well as rod samples were cut are shown in Fig. 1.

Table 1. Composition of commercial FeCrAl stainless steels wt%

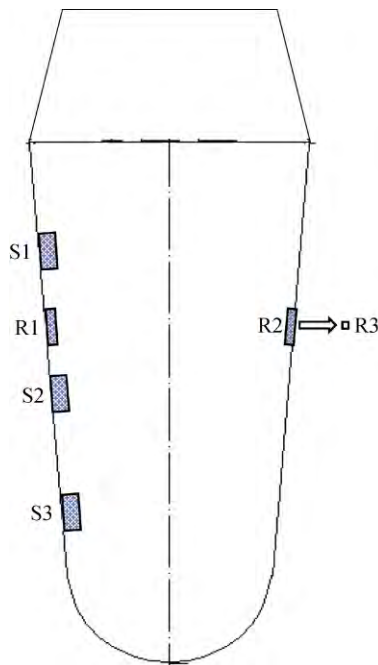| Brand	C	Si	Mn	S	P	Cr	Al	RE
0Cr20Al6	≤ 0.03	≤ 0.6	—	≤ 0.015	≤ 0.025	19.0−21.0	5.0−6.0	Proper
JFE20-5USR	0.005	0.1	0.1	—	—	20.0	5.5	0.08
JFE20-3USR	0.003	0.1	0.1	—	—	18.0	3.4	0.08

Fig. 1. Positions from where scraps and rod samples were cut.

Scraps S1, S2, and S3 were sampled and uniformly mixed for chemical analysis; the results are listed in Table 2. "Als" denotes Al in the solid solution state. Two rods labeled R1 and R2 with dimensions φ5 mm × 10 mm and φ3 mm × 10 mm, respectively, were cut from the dense parts of

the ingot. Sample R1 was cleaned and prepared for analysis of O and N. The chemical compositions of the four melts are shown in Table 2. A new sample labeled R3 with dimensions φ3 mm × 2 mm was cut from R2 and prepared for DSC testing.

The macro segregation of Al, Cr, Si, and Mn in ingot B was simulated using the Pro-CAST simulation software for a pouring rate of 0.05 kg/s and a pouring temperature 1560°C, consistent with real melting and casting experiment parameters. This work was conducted to investigate if obvious differences in content existed among the different sampling positions of S1, S2, S3, and R3 in Fig. 1. The macro segregation of ingot B described in Table 2 is presented in Fig. 2.

In Fig. 2, the maximum and minimum Al contents for ingot B are 4.4061wt% and 4.3880wt%, respectively. These two values are very close to each other; thus, the content variation among S1, S2, S3, R1, and R3 in Fig. 1 should be small. Similarly, Cr, Si, and Mn also distributed uniformly in ingot B. Thus, the difference in composition among the different sampling positions in Fig. 1 was small, so the average compositions of S1, S2, and S3 could represent the composition of R3, which would be used for DSC testing. The distributions of the elements in the other three ingots were also analyzed using the same method, and very similar results were obtained.

Table 2. Chemical composition of four FeCrAl steel ingots wt%

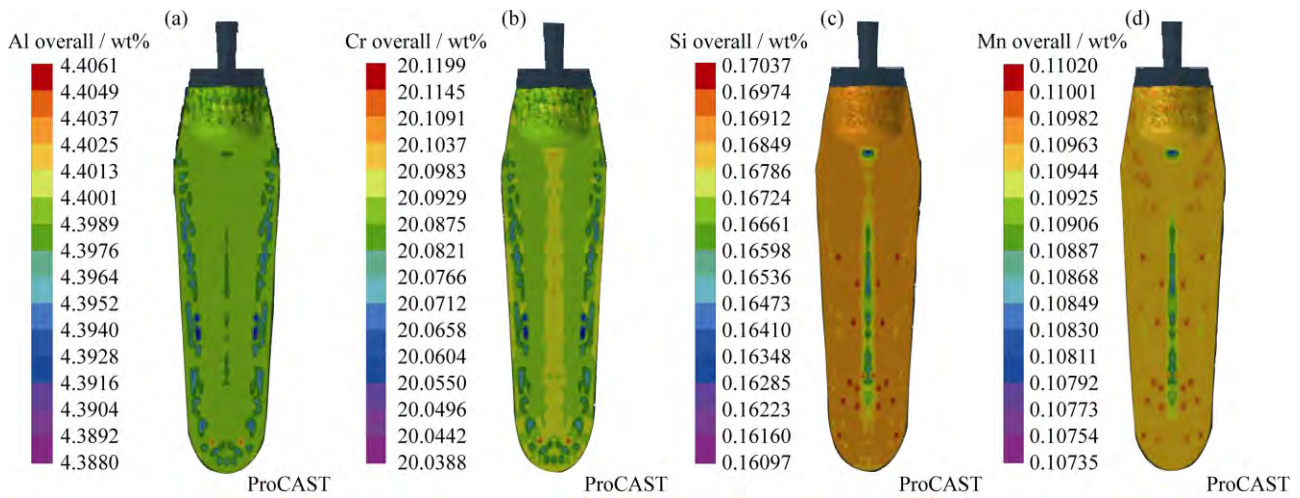| Sample	C	Si	Mn	S	P	Cr	Als	N	O
A	0.017	0.033	0.019	0.0050	0.0077	20.01	3.58	0.0075	0.0014
B	0.023	0.170	0.110	0.0041	0.0056	20.09	4.39	0.0100	0.0018
C	0.015	0.033	0.018	0.0045	0.0072	20.00	5.84	0.0044	0.0017
D	0.022	0.210	0.110	0.0049	0.0052	19.96	6.49	0.0170	0.0025

Fig. 2.   Macro-segregation of ingot B: (a) Al distribution; (b) Cr distribution; (c) Si distribution; (d) Mn distribution.

2.2. Procedure for DSC testing

The differential scanning calorimeter used in this study was Netzsch DSC 404F3, which was calibrated in advance using high-purity metal. The sample was placed into an alumina crucible, which was subsequently inserted into the sample chamber. The sample chamber was evacuated to pressure less than 10^{-3} Pa and then backfilled with 99.999% Ar to a pressure approximately 10^5 Pa. This evacuation-backfilling operation was repeatedly performed three times. An empty alumina crucible was used as the reference. After the final back filling with Ar, DSC curves were obtained according to the flow chart in Fig. 3.
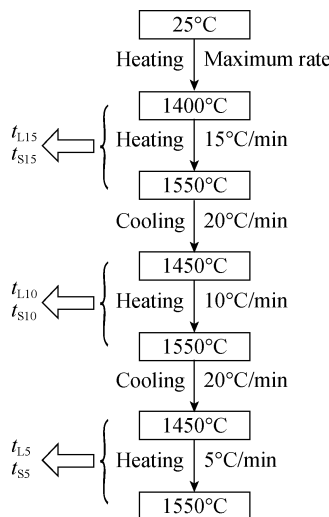

Fig. 3.   Flow chart of the heating and cooling procedure.

t_L and t_S were obtained via a heating process instead of a cooling process to eliminate the influence of solidification supercooling and thereby provide more reliable results. As outlined in Fig. 3, each of the four samples was tested at three different heating rates of 15, 10, and 5°C/min. Three corresponding DSC curves for the same sample but with different heating rates were obtained. On the basis of these curves, t_L and t_S for each sample were determined at different heating rates.

Then the curve of solidus (or liquidus) versus heating rate was plotted and the quantitative relations between solidus (or liquidus) and heating rate were determined. More importantly, solidus and liquidus without the disturbance of heating rate were obtained by extrapolation method.

2.3. DSC results

DSC curves of the four samples with different heating rates are shown in Fig. 4. In Fig. 4, the onset and peak temperature of each DSC curve were regarded as the solidus (t_S^{DSC}) and liquidus (t_L^{DSC}) temperature determined by DSC, respectively [10−13]. The corresponding results are listed in Tables 3 and 4, respectively.

The results in Tables 3 and 4 indicated that both the solidus and liquidus temperatures increased with an increase in heating rate v [6]. Therefore, the effect of heating rate on the DSC results should be carefully considered. t_S^{DSC} and t_L^{DSC} in Tables 3 and 4 were plotted against v, respectively. Accordingly, the relations between t_S^{DSC} as well as t_L^{DSC} and v were obtained. Based on these relations, the solidus and liquidus temperatures at $v = 0$ were determined and regarded as the final results of DSC experiments, as shown in Table 5. The solidus and liquidus temperatures in Table 5 are more accurate and could be regarded as "criteria" to assess the accuracy of t_L and t_S calculated by TC and by empirical formulae.
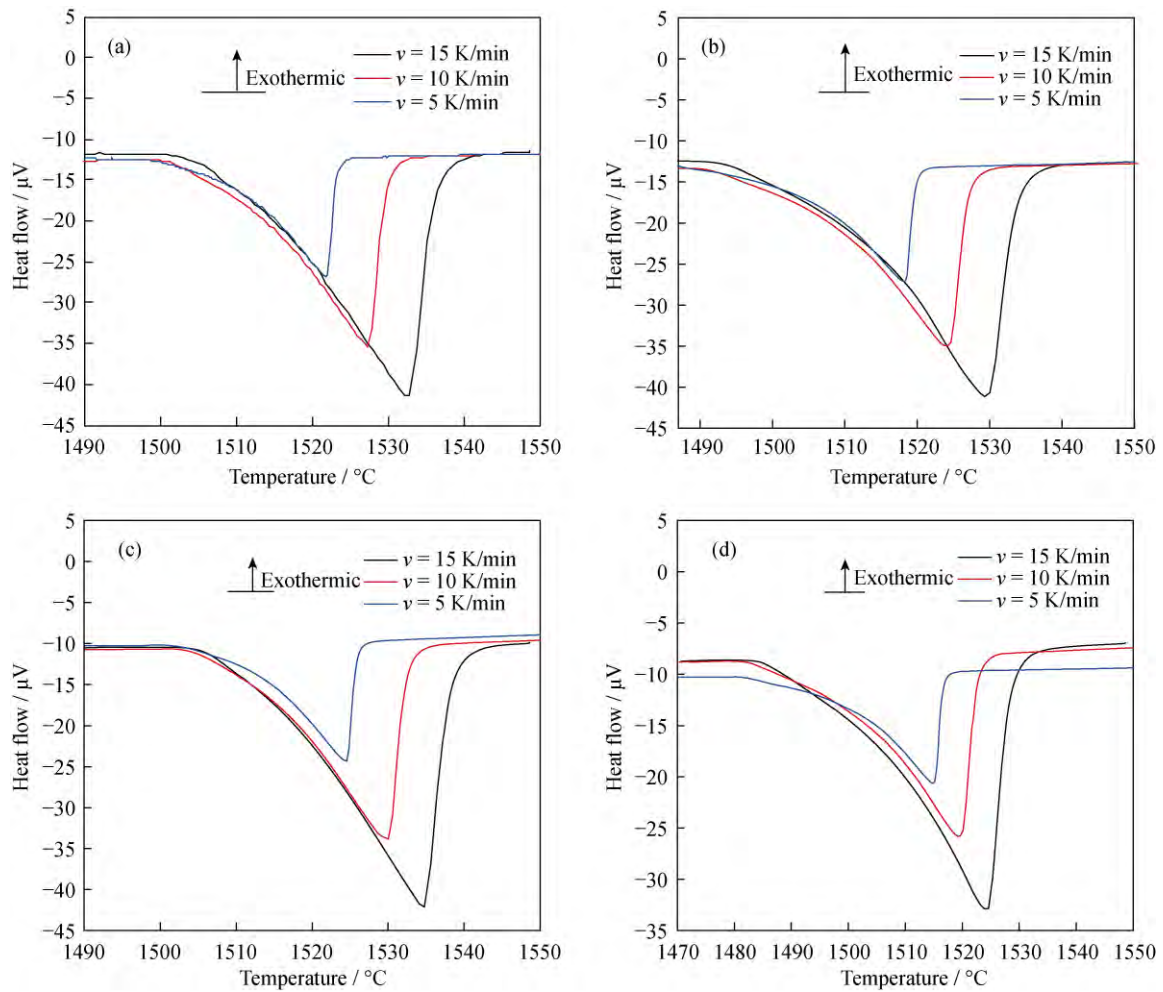
Fig. 4. DSC curves of the four samples: (a) sample A; (b) sample B; (c) sample C; (d) sample D.

Table 3. Solidus temperatures determined at different heating rates °C

Sample	Heating rate / (K·min⁻¹)		
	5	10	15
A	1508.3	1509.3	1510.4
B	1502.2	1504.6	1506.8
C	1510.5	1511.7	1513.0
D	1498.5	1499.8	1501.3

Table 4. Liquidus temperatures determined at different heating rates °C

Sample	Heating rate / (K·min⁻¹)		
	5	10	15
A	1521.7	1527.3	1532.8
B	1518.1	1524.2	1529.3
C	1524.6	1530.0	1534.8
D	1514.9	1519.2	1523.9

Table 5. $t_S^{DSC} - v$ and $t_L^{DSC} - v$ relations, fitting degrees and the final results

Sample	$t_S^{DSC} - v$ relation	Fitting degree	t_S^{DSC} / °C	$t_L^{DSC} - v$ relation	Fitting degree	t_L^{DSC} / °C
A	$t_S^{DSC} = 1507.2 + 0.21v$	0.9985	1507.2	$t_L^{DSC} = 1516.3 + 1.09v$	0.9992	1516.3
B	$t_S^{DSC} = 1499.9 + 0.46v$	0.9987	1499.9	$t_L^{DSC} = 1512.7 + 1.12v$	0.9954	1512.7
C	$t_S^{DSC} = 1509.2 + 0.25v$	0.9989	1509.2	$t_L^{DSC} = 1519.6 + 1.02v$	0.9970	1519.6
D	$t_S^{DSC} = 1497.1 + 0.28v$	0.9966	1497.1	$t_L^{DSC} = 1510.3 + 0.90v$	0.9989	1510.3

3. Analysis of liquidus by different methods

The liquidus temperatures were calculated using TC (denoted by t_L^{TC}) and empirical formulae (denoted by t_L^{cal}) separately. These two calculation results were subsequently compared with the DSC results to evaluate the accuracy of these calculations.

3.1. Comparison between t_L^{TC} and t_L^{DSC}

We used TC in conjunction with the TCFE7 database to calculate the liquidus temperatures of the four samples. t_L^{TC} and the corresponding deviations from t_L^{DSC} (denoted by Δt_L^{TC}) are listed in Table 6. The average deviation ($\overline{\Delta t_L^{TC}}$) between t_L^{TC} and t_L^{DSC} in Table 6 is 12.11°C. Thus, the TC software could be used to calculate the approximate t_L and t_S for FeCrAl steel.

Table 6.   Comparison between t_L^{TC} and t_L^{DSC} °C

Sample	t_L^{DSC}	t_L^{TC}	Δt_L^{TC}	$\overline{\Delta t_L^{TC}}$
A	1516.31	1527.50	11.19	
B	1512.68	1525.68	13.00	12.11
C	1519.57	1530.80	11.20	
D	1510.34	1523.39	13.05	

3.2. Comparison between t_L^{cal} and t_L^{DSC}

The liquidus temperatures were obtained through empirical formulae. Expressions (1)−(6) appear to be suitable for calculating the liquidus temperatures of FeCrAl stainless steel [14].

$$t_L^{cal} = 1535 - 73[\%C] - 3[\%Mn] - 12[\%Si] - 28[\%P] - 30[\%S] - [\%Cr] - 3[\%Al] \tag{1}$$

$$t_L^{cal} = 1534 - 80[\%C] - 4[\%Mn] - 14[\%Si] - 35[\%P] - 1.4[\%Cr] - 3.4[\%Al] \tag{2}$$

$$t_L^{cal} = 1535 - 80[\%C] - 14[\%Si] - 4[\%Mn] - 35[\%P] - 35[\%S] - 1.4[\%Cr] - 3.4[\%Al] \tag{3}$$

$$t_L^{cal} = 1536 - 8[\%C] - 7.6[\%Si] - 3.9[\%Mn] - 33.4[\%P] - 38[\%S] - 1.3[\%Cr] - 3.6[\%Al] \tag{4}$$

$$t_L^{cal} = 1536 - 251[\%C] - 12.3[\%Si] - 6.8[\%Mn] - 123.4[\%P] - 183.9[\%S] - 1.4[\%Cr] - 3.6[\%Al] \tag{5}$$

$$\begin{cases} t_L^{cal} = 1536 - 76.77(C_C + F) - 6.89(C_C + F)^2 \\ F = F_{Si} + F_{Mn} + F_{Al} + F_{Cr} \\ F_{Si} = C_{Si}\left[1 - 0.8384 + (3.544 \times 10^{-3} C_{Si})\right] \\ F_{Mn} = C_{Mn}\left[1 - 0.9433 - (2.6 \times 10^{-4} C_{Mn})\right] \\ F_{Cr} = C_{Cr}\left[1 - 0.9713 - (6.84 \times 10^{-4} C_{Cr})\right] \\ F_{Al} = C_{Al}\left[1 - 1.0011 - (2.8154 \times 10^{-5} C_{Al})\right] \end{cases} \tag{6}$$

In formula (6), C_i is the mass content of alloying element i, F_i is concentration functions of alloying elements in ferrite. The liquidus temperatures t_L^{cal} obtained from empirical formulae, and their deviations from the corresponding DSC results are listed in Tables 7 and 8, respectively.

Table 7.   Liquidus temperatures obtained by formulae (1)−(6)
°C

Sample	Formulae					
	(1)	(2)	(3)	(4)	(5)	(6)
A	1502.2	1491.7	1492.5	1496.2	1488.4	1510.8
B	1497.4	1486.1	1485.9	1491.8	1482.0	1508.7
C	1495.6	1484.2	1484.0	1488.1	1481.0	1511.0
D	1490.8	1478.7	1478.5	1484.1	1474.3	1508.2

Table 8.   Deviations between t_L^{cal} and t_L^{DSC} °C

Sample	Formulae					
	(1)	(2)	(3)	(4)	(5)	(6)
A	−14.1	−24.6	−23.8	−20.1	−27.9	−5.5
B	−15.5	−26.8	−27.0	−21.1	−30.9	−4.0
C	−24.0	−35.4	−35.6	−31.5	−38.6	−8.6
D	−16.7	−28.8	−29.0	−23.4	−33.2	−2.1

As evident from the results in Table 8, the t_L^{cal} values obtained using formula (6) turned out to be more accurate than the TC results; thus, formula (6) could be better than TC software for calculating the liquidus temperature of FeCrAl stainless steel.

4. Determination of solidus temperature

The liquidus temperatures of steels can be calculated using formulae or the TC software; however, the solidus temperatures cannot be obtained so easily or accurately. Fortunately, the curve of solid phase fraction (f_S) vs. temperature (t) can be conveniently obtained using TC. In conjunction with DSC results, this f_S−t curve may provide a new method for determining solidus temperatures using TC. To obtain reliable results, the solidification route of FeCrAl stainless steel during and immediately after equilibrium solidification should be specified in advance.

4.1. Solidification route of FeCrAl stainless steel

The main components of typical FeCrAl stainless steel are 18wt%−21wt% [Cr] and 3wt%−6wt% [Al] (Table 1). This composition is beyond the stable region of γFe, which shrinks at temperatures above ~1000°C and finally disappears when the temperature exceeds ~1400°C. The solidus

temperatures of FeCrAl steel are higher than 1450°C (Table 5); thus, the Fe–Cr–Al ternary system should be complete αδFe. In addition, the contents of austenite stabilizer (C ≤ 0.03wt%, Mn ≤ 0.1wt%) are quite low, so the solidification route of FeCrAl stainless steel should be L → L + δ → δ, with no γ phase during or after solidification [15−17].

4.2. Temperature investigation under Scheil model

When the solid fraction almost reaches 1, the solidification is complete and the corresponding temperature should be regarded as t_S. Therefore, we here investigated the temperature corresponding to $f_S \rightarrow 1$ using f_S–t curves calculated with TC under the modified Scheil model [18], which is

widely used for conventional ingot casting. Because this model takes the solid diffusion of some interstitial atoms (such as C and N) into consideration, it is regarded to be more accurate than the traditional Scheil model in describing the solidification behavior of real ingots. According to the analysis described in section 4.1, f_S should actually be the ferrite phase fraction during the solidification of FeCrAl stainless steel.

This research mainly focused on the relationship between f_S and t_S; thus, the tiny amounts of impurity elements (O, N, S, and P) listed in Table 2 were not taken into consideration. The f_S–t curve for each sample, as calculated under the modified Scheil model is shown in Fig. 5.
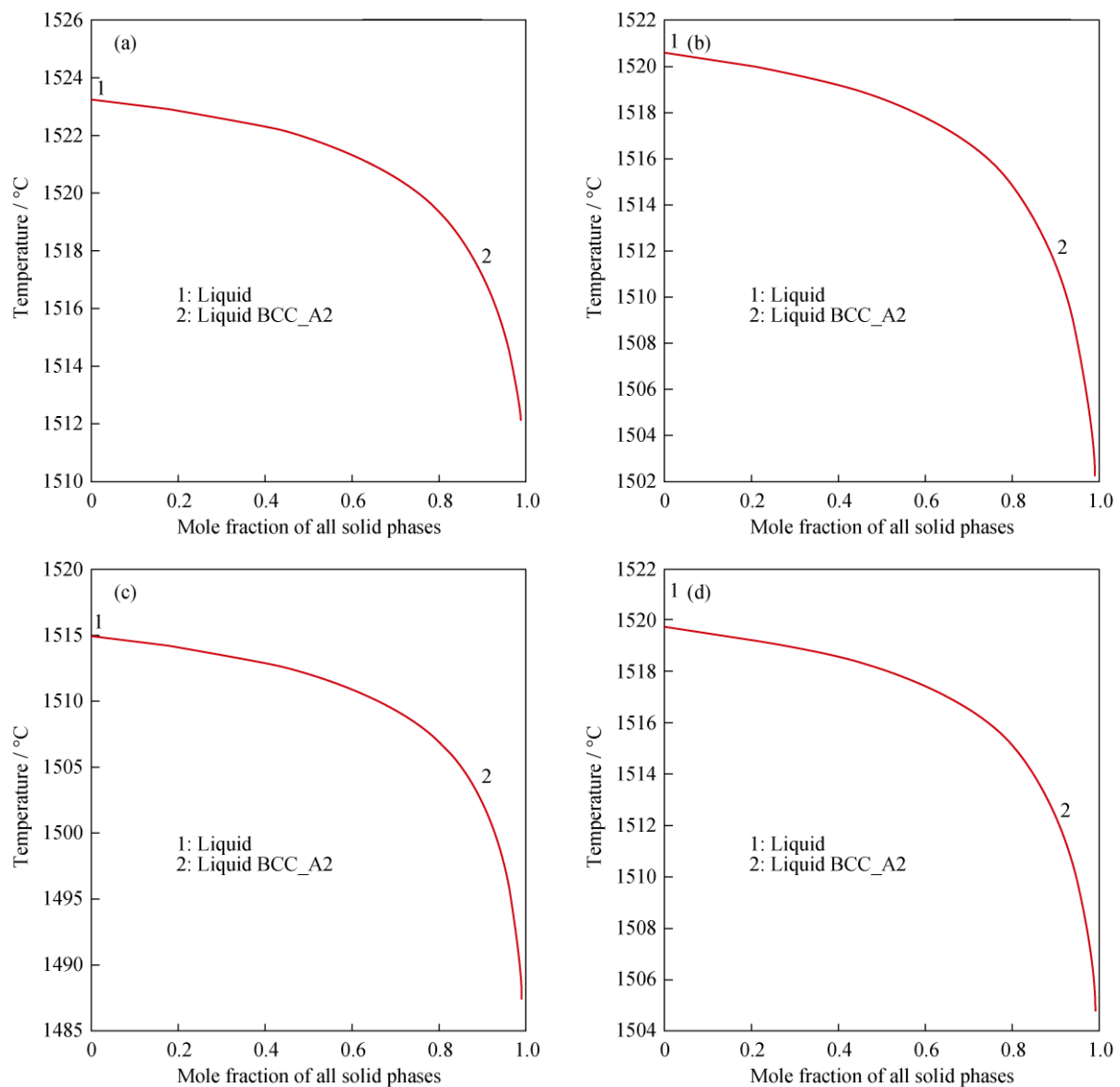

Fig. 5. f_S–t curves of the four samples under Scheil model: (a) sample A; (b) sample B; (c) sample C; (d) sample D.

Fig. 5 clearly indicates that FeCrAl stainless steel with the composition listed in Table 1 solidifies with the forma-

tion of a single ferrite and no austenite phase during Scheil solidification. This result is consistent with the analysis pre-

sented in section 4.1. Furthermore, all of the f_S–t curves ended at $f_S = 0.99$. This solid fraction may represent the end of solidification in TC. Therefore, the temperatures at $f_S = 0.99$ (denoted by t_S^{TC}) were obtained from Fig. 5 and compared to the corresponding solidus temperatures determined by DSC (Table 5) to assess the reliability of the former results according to $\Delta t_S = t_S^{TC} - t_S^{DSC}$. The results are listed in Table 9.

Table 9. Temperatures at $f_S = 0.99$ and deviations from the DSC results °C

Sample	t_S^{TC}	t_S^{DSC}	Δt_S
A	1511.9	1507.2	4.7
B	1502.2	1499.9	2.3
C	1504.8	1509.2	4.4
D	1487.2	1497.1	9.9

The results in Table 9 clearly indicate that, with the exception of the Δt_S value for sample D, the ΔT_S values are less than 5°C, indicating that the temperature at $f_S = 0.99$ should be a reasonable solidus temperature. The deviation in the case of sample D was 10°C. This result may be erroneous, or it may arise from the substantially greater Al content (6wt% or more) in this sample. Therefore, the determination of t_S using this method should be conducted with caution for samples with Al contents of 6wt% or more.

The reason the temperature at $f_S = 0.99$ matches so well with the solidus temperature determined by DSC is explained as following. The solidification process of ingot casting is well described by the Scheil model; thus, the components in different regions of ingots should be layered. At the end of solidification, the solid phase was in local equilibrium with the last drop of the liquid phase. The amount of this last drop of liquid was probably 1% in this study (but may be different for other alloy systems), and the corresponding temperature could be regarded as the solidus temperature, which could be an indicator of the end of solidification.

If solid diffusion during the cooling of the ingot can be neglected, then, the heating process during DSC testing can be regarded as the reverse of the solidification process. The temperature at which this 1% solid completely melts and maintains local equilibrium with the remaining 99% of the solid can be regarded as the solidus temperature with heating rate $v = 0$ as the guarantee for local equilibrium [19]. Thus, the temperature at $f_S = 0.99$ in the TC results calculated using the modified Scheil model matches well with the solidus temperature determined by DSC at $v = 0$.

5. Conclusions

(1) For FeCrAl stainless steel, the deviations between the liquidus temperatures determined using a certain empirical formula and those determined by DSC were less than 10°C, whereas the deviations between the TC and DSC results were relatively larger, with average of approximately 12.11°C. Thus, the formula may represent a better choice for calculating the liquidus temperature of FeCrAl stainless steel.

(2) The solidus temperatures of FeCrAl stainless steel was determined from the curve of the solid phase fraction vs. temperature (f_S–T curve), which was calculated under the modified Scheil model using TC. According to the DSC results, the temperature corresponding to the point $f_S = 0.99$ could be reasonably selected as the solidus temperature for FeCrAl stainless steel, where most of the deviations from the DSC results were less than 5°C.

Acknowledgements

References

[1] W.J. Quadakkers and M.J. Bennett, Oxidation induced lifetime limits of thin walled, iron based, alumina forming, oxide dispersion strengthened alloy components, *Mater. Sci. Technol.*, 10(1994), p. 126.

[2] D.V. Satyanarayana and M.C. Pandey, The role of active elements in Fe–Cr–Al alloys for heating applications, *Bull. Mater. Sci.*, 18(1995), No. 3, p. 207.

[3] L.M. Shen and J.S. Lu, Overview of researching of the carrier used for automobile gas purfier, *Shanghai Iron Steel Res.*, (2004), No. 1, p. 35.

[4] S. Matsumoto, Recent advances in automobile exhaust catalyst, *Catal. Surv. Jpn.*, 1(1997), p. 111.

[5] J. Miettinen and A.A. Howe, Estimation of liquidus temperatures for steels using thermodynamic approach, *Ironmaking steelmaking*, 27(2000), No. 3, p. 212.

[6] R.I. Wu and J.H. Perepezko, Liquidus temperature determination in multicomponent alloys by thermal analysis, *Metall. Mater. Trans. A*, 31(2000), p. 497.

[7] V.G. Rivlin and G.V. Raynor, Critical evaluation of constitution of aluminum–chrominum–iron system, *Int. Met. Rev.*, (1980), No. 4, p. 139.

[8] D.L. Hu and F. Zhang, *Ternary Alloy Phase Diagrams*, Northwestern Polytechnical University Press, Xi'an, 1995, p. 117.

[9] A.A. Howe, Estimation of liquidus temperatures for steels, *Ironmaking Steelmaking*, 15(1998), No. 3, p. 134.

1148

Int. J. Miner. Metall. Mater., Vol. 22, No. 11, Nov. 2015

[10] K. Gryc, B. Smetana, and M. Zaludová. Determination of the solidus and liquidus temperatures of the real-steel grades with dynamic thermal-analysis methods, *Mater. Technol.*, 47(2013), No. 5, p. 569.

[11] M.J. Cieslak, T.J. Headley, G.A. Knorovsky, A.D. Romig, Jr., and T. Kollie, A comparison of the solidification behavior of INCOLOY 909 and INCONEL 718, *Metall. Trans. A*, 21(1990), p. 479.

[12] C.V. Robino, J.R. Michael, and M.J. Cieslak, Solidification and welding metallurgy of Thermo-Span alloy, *Sci. Technol. Weld. Joining*, 2(1997), No. 5, p. 220.

[13] W. Banda, G.A. Georgalli, C. Lang, and J.J. Eksteen, Liquidus temperature determination of the Fe–Co–Cu system in the Fe-rich corner by thermal analysis, *J. Alloys Compd.*, 461(2008), No.1-2, p. 178.

[14] J.X. Chen, *Frequently Used Data and Diagrams in Steel Making*, Metallurgical Industry Press, Beijing, 2010, p. 511.

[15] P. Presoly, R.Piererr, and C. Bernhard, Identification of defect prone peritectic steel grades by analyzing high temperature phase transformations, *Metall. Mater. Trans. A*, 44(2013), No. 12, p. 5337.

[16] A. Kagawa and T. Okamoto, Influence of alloying elements on temperature and composition for peritectic reaction in plain carbon steels, *Mater. Sci. Technol.*, 2(1986), p. 997.

[17] P. Presoly, G.M. Xia, P. Reisinger, and C. Bernhard, Continuous casting of hypo-peritectic steels: mould thermal monitoring and DSC-analysis, *Berg Hüttenmänn. Monatsh.*, 159(2014), No. 11, p. 430.

[18] P. Schaffnit, C. Stallybrass, J. Konrad, Frank Stein, and M. Weinberg, A Scheil–Gulliver model dedicated to the solidification of steel, *Calphad*, 45(2015), p. 184.

[19] M. Ohno, D. Mirkovic, and R. Schmid-Fetzer, Liquidus and solidus temperatures of Mg-rich Mg–Al–Mn–Zn alloys, *Acta Mater.*, 54(2006), No. 15, p. 3883.